Superlattices and Microstructures 130 (2019) 321–331

Contents lists available at ScienceDirect

Superlattices and Microstructures

journal homepage: www.elsevier.com/locate/superlattices

Room-temperature synthesis and optical properties of nanostructured Ba-Doped ZnO thin films

C.C. Okorieimoh [a], Ugochi Chime [a], Agnes C. Nkele [a], Assumpta C. Nwanya [a,b,c], Itani Given Madiba [b,c], A.K.H. Bashir [b,c], Subelia Botha [d], Paul U. Asogwa [a], Malik Maaza [b,c], Fabian I. Ezema [a,b,c,e,*]

[a] Department of Physics and Astronomy, University of Nigeria, Nsukka
[b] Nanosciences African Network (NANOAFNET), iThemba LABS-National Research Foundation, 1 Old Faure Road, Somerset West 7129, P.O. Box 722, Somerset West, Western Cape Province, South Africa
[c] UNESCO-UNISA Africa Chair in Nanosciences/Nanotechnology, College of Graduate Studies,University of South Africa (UNISA), Muckleneuk Ridge, P.O. Box 392, Pretoria, South Africa
[d] Electron Microscope Unit, University of the Western Cape, South Africa
[e] Department of Physics, Faculty of Applied and Natural Sciences, Coal City University, Enugu, Nigeria

ARTICLE INFO

Keywords:
BaZnO
Thin films
SILAR technique
Optical properties
SEM
XRD

ABSTRACT

Zinc oxide films with and without barium-doping have been prepared by the SILAR technique at different concentrations (1 mol%, 3 mol%, 5 mol% and 7 mol%) of Ba content on glass slides. The effects of the concentration of barium doped zinc oxide (BaZnO) were characterized using x-ray difffractometry (XRD), scanning electron microscopy (SEM), energy dispersive x-ray spectroscopy (EDX), transmission electron microscopy (TEM), selected area electron diffraction (SAED) techniques, ultraviolet–visible spectroscopy and photoluminescence (PL) studies. The structural studies using XRD plots confirmed the polycrystalline nature of ZnO films. The Ba doped ZnO films deposited were found to have strong orientation at (002) lattice plane which exhibited polycrystalline hexagonal wurtzite structure. TEM and SAED results confirmed the morphological and structural properties of the films. The SEM showed that the grain size of the films increased as a result of increase in the concentration of barium doping. EDX results confirmed the elemental presence of the films. An increase in the Ba concentration showed a decrease in the optical band gap values between 3.41 eV and 3.19 eV. PL studies confirmed the presence of defects in the ZnO films.

1. Introduction

Zinc oxide (ZnO) has been synthesized and characterized by researchers for many years due to its unique properties of wide band-gap, optical transparency, high binding energy of excitons and optical transparency in the visible region [1]. At 300 K, ZnO as a semiconductor has a wide band gap of 3.37 eV [2]. Due to its wide band gap, ZnO thin films have been utilized in optoelectronic devices [3–6], photo-thermal conversion systems, blue/UV light emitter devices, solid state sensors, transparent electrodes, hetero-junction solar cells etc. [7–12]. The applications of undoped zinc oxide thin films are limited. This has led to the addition of dopant ions

* Corresponding author.
E-mail address: fabian.ezema@unn.edu.ng (F.I. Ezema).

https://doi.org/10.1016/j.spmi.2019.05.010
Received 30 January 2019; Received in revised form 15 April 2019; Accepted 7 May 2019
Available online 8 May 2019

to ZnO thin films to obtain varying melting points, band gaps and optical absorbance via different deposition techniques.

Specialized techniques such as RF magnetron sputtering [13], chemical vapour deposition [14], chemical bath deposition [15], pulsed laser deposition [16], spray pyrolysis [17], sol-gel process [18,19], chemical co-precipitation [20], hydrothermal [21], ultrasonic irradiation assisted solution route [22], solid-state reaction [23], successive ionic layer adsorption and reaction (SILAR) [24,25] etc. have been employed to synthesize ZnO nanostructured thin films. SILAR technique is therefore a preferred deposition technique due its low cost, uniform film deposition and simplicity. Furthermore, this technique requires low temperatures and facilitates large-area deposition [26]. ZnO doped with Ba is a technological material used in varistors and in the guiding layers of liquid sensors [27]. Barium was chosen as a dopant because of its stable current-voltage properties, useful for producing optoelectronics and miniaturized devices in the nanoscale [28]. Despite having the same valence electron with the host atom, the ionic radius of barium makes it able to substitute itself into the lattice of the ZnO during the doping process. The doping of ZnO with Ba creates crystalline structures with smooth surfaces and low density, which also have the ability to absorb internal stress [29]. Doping with barium helps to reduce the energy bandgap and increase the separation of charges in ZnO nanoparticles [30].

This paper investigates the effect of varying percentages of barium (Ba) as a doping material on zinc oxide (ZnO) thin films synthesized by a simple yet effective SILAR technique, using $ZnSO_4{\cdot}2H_2O$ and $BaCl_2$ as precursor materials. Comprehensive discussion from the XRD, TEM, SAED, SEM, EDX, UV–vis spectroscopy and PL results have been presented. The obtained results would be beneficial in optoelectronics device applications.

2. Details of experiments

2.1. Substrate cleaning

For deposition of ZnO films on glass slides, SILAR technique was adopted. The clean glass slides (micro slide-25.4 mm wide × 76.2 mm lengths and thickness 1mm-1.2 mm) were soaked in acetone (to degrease the substrates from any possible stains) for 30 min, ultrasonicated for 20 min and rinsed in distilled water. Finally, they were dried in a thermo-blast furnace for 20 min at 60 °C. The cleaned glass slides were gently safe guarded in a clean glass slide pack and ready for use.

2.2. Synthesis procedure

For depositing the undoped ZnO film, 0.8 M of hydrated zinc sulphate ($ZnSO_4{\cdot}2H_2O$) was prepared with aqueous ammonia (NH_4OH, 29%) and 50 ml of distilled water. The aqueous solution was then stirred thoroughly on a magnetic stirrer for about 20 min to allow for complete dissolution in order to produce a colourless aqueous solution of $[Zn(NH_3)_4]^{2+}$ (Zinc(II) tetra-amine ion) cationic precursor. The aqueous ammonia added to the resultant mixture helped to moderate the pH solution to 8.1. For the growth of ZnO (intrinsic semiconductor) films, 40 cycles were carried out in each case.

For the synthesis of Ba-doped ZnO (BaZnO) (extrinsic semiconductor) thin films, a measured amount of barium chloride ($Bacl_2$) was added to the initial solution in a separate beaker. In order to determine the effect of varying percentages of barium (Ba) as a dopant on ZnO thin films, we conducted the experiments at five different concentrations. Ba^{2+} ions were added to the deposition beakers at 1 mol %, 3 mol%, 5 mol% and 7 mol%.

The summary of the procedure for depositing the ZnO films at 40 cycles are:

The clean glass slides (substrates) were dipped in the complex aqueous of zinc (II) tetra-amine ion $[Zn(NH_3)_4]^{2+}$ (cationic precursor) kept at room temperature for 30 s. Immediately the precipitates were formed, the substrates were immersed in distilled water at room temperature for 30 s. The substrates were dipped in hot distilled water bath maintained at 70 °C–80 °C for 30 s to adsorb oxygen and generate ZnO. The glass slides were afterwards dipped for 30 s in distilled water at room temperature in order to separate the counter ions $S0_4^{2-}$ from loosely precipitated $Zn(OH)_2$ grains as shown in Fig. 1.

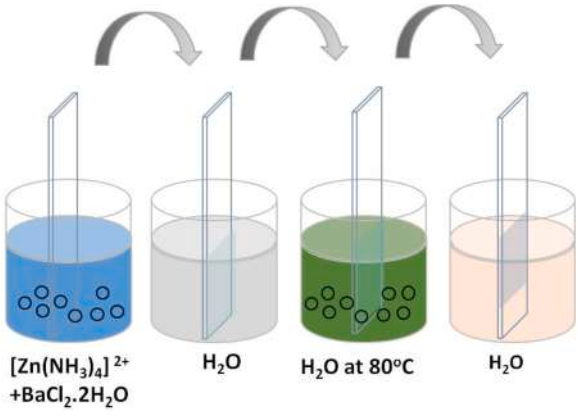

Fig. 1. Experimental set up for the SILAR technique adopted.

2.3. Reaction equations

From equation (1)–(5), it exemplifies a chemical reaction connected with both the undoped and doped process:
Un-doped process:

$$ZnSO_4.2H_2O + 2NH_4OH \rightarrow Zn(OH)_2 + (NH_4)_2SO_4 + 2H_2O \quad (1)$$

$$Zn(OH)_2 + 4NH_3.H_2O \rightarrow \left[Zn(NH_3)_4\right]^{2+} + 2OH^- + 4H_2O \quad (2)$$

It was deduced from the process of the anionic reaction, complex aqueous solution of zinc (II) tetra-amine ions, broke up with Zn $(OH)_2$ precipitation:

$$\left[Zn(NH_3)_4\right]^{2+} + 4H_2O \rightarrow Zn(OH)_2 \downarrow + 4NH_4 + 2OH^- \quad (3)$$

Therefore,

$$Zn(OH)_2 \rightarrow ZnO + H_2O \quad (4)$$

Doped process:

$$\left[Zn(NH_3)_4\right]^{2+} + BaCl_2.2H_2O \rightarrow \left[ZnBa(NH_3)_4\right]^{2+} + Cl_2 + 2H_2O \quad (5)$$

2.4. Characterisation

XRD, TEM, SAED, SEM, EDX and UV–Vis analyses were performed in order to figure out the structural, morphological, elemental compositions and optical analysis of the undoped and doped ZnO films. A D8 advanced X-ray diffractometer was used to obtain the crystal structures of the films over a scanning range of $2\theta = 10 - 90^\circ$ while a Zeiss scanning electron microscope was used to obtain the film morphologies. TEM micrographs and SAED patterns were obtained using a Tecnai G^2 F20 S-Twin High Resolution Transmission Electron Microscope (HRTEM) operated at 200 kV. The optical analysis of the films was determined using Shumalzu UV-1800 spectrophotometer at room temperature over the range of 200–1000 nm. Photoluminescence (PL) spectroscopy was carried out using an F-7000 FL spectrophotometer model at a chopping speed of 40 Hz.

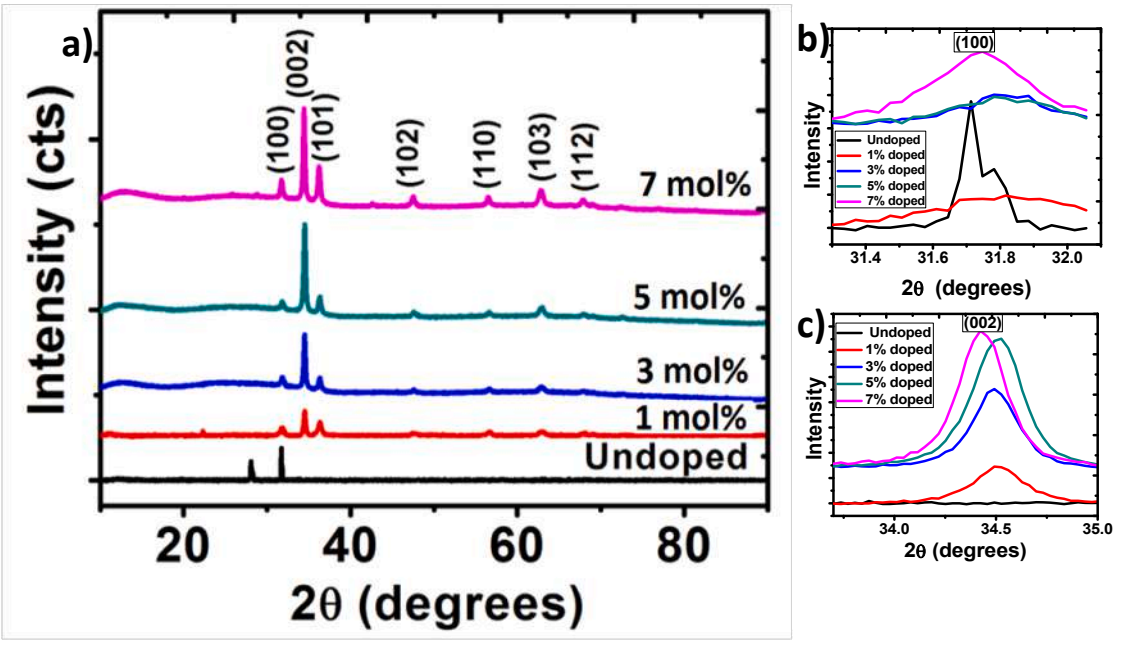

Fig. 2. The XRD pattern for undoped ZnO and Ba-doped ZnO a) for all the diffraction peaks b) for the (100) diffraction plane c) for the (002) diffraction plane.

3. Results of the experiment and discussion

3.1. Structural characterisation

Crystallographic analysis of ZnO films was determined using XRD technique. Fig. 2 shows the XRD plots of the undoped ZnO (intrinsic semiconductor) and barium-doped ZnO (extrinsic semiconductor) films at different dopant concentrations. Several diffraction peaks were noticed as in Fig. 2(a). These diffraction peaks show the polycrystalline nature of the films [31].

The x–ray diffractograms were used to confirm the presence of the dopant: barium in the lattice plane of ZnO. For the Ba-doped ZnO (BaZnO) (extrinsic semiconductor) films, prominent peaks were showed at $2\theta = 31.7^{\circ}$, 34.5°, 36.3°, 47.6°, 56.7°, 62.8° and 67.8° which corresponds to (100), (002), (101), (102), (110), (103) and (112) lattice planes respectively compared to the undoped ZnO films which showed less number of peaks. An increase in Ba concentration showed an increase in peak intensity at the (002) plane for all the deposited films. The undoped film recorded maximum peak intensity at the (100) plane with no peak seen at the (002) plane. The lattice planes at (100) and (002) have been zoomed in Fig. 2(b and c) to show the peak broadening and slight peak shift experienced upon doping with barium. The most intense peak at the (002) plane has been put as Fig. 2(c) to show the peak broadening and evidence of peak shifting due the dopants. This result shows that Ba atoms act as donors in ZnO films thereby donating extra valence electrons to the conduction band of the semiconductor. This provided excess electrons to the undoped ZnO thereby making it an n-type semiconductor.

Table 1 shows the different parameters obtained from the XRD plots. Scherrer's equation was used to obtain the average crystallite size [32,33]:

$$D = \frac{0.9\lambda}{\beta cos\theta} \tag{6}$$

Where λ is the wavelength, θ is the Bragg's diffraction angle and β is the full width at half maximum. The undoped crystallites presented a much higher crystallite size than those of the Ba-doped samples. The crystallite sizes of the ZnO at different dopant concentrations ranged from 30.4 to 33.6 nm. The separation between parallel atomic planes referred to as inter-planar distance, d, was obtained using equation (7) [34].

$$d = {}^{\lambda}/_{2\sin\theta} \tag{7}$$

The lattice strain, ε, which is due to deformities and inhomogeneity of the film was obtained using equation (8) [35].

$$\varepsilon = {}^{\beta}/_{4\tan\theta} \tag{8}$$

The dislocation density was obtained using equation (9) [36].

$$\delta = \frac{1}{D^2} \tag{9}$$

There was a sharp decrease in crystallite size from 82.22 nm for the undoped ZnO to 30.43 nm for Ba-doped ZnO at 1 mol% owing to the dopant introduction. However, slight variations in the crystallite sizes have been observed at different dopant concentrations of the films as seen in Table 1.

Transmission electron microscopy (TEM) has been adopted to confirm the shape, size and hexagonal crystal structure of the deposited films. The TEM micrographs and SAED patterns are shown in Fig. 3. TEM technique was used to further explain the morphology of the barium-doped nanoparticles. The particles showed capsule-like morphology with similar sizes as the 31 nm average calculated from the Debye-Schrerrer's equation. Smaller particles with sizes less than 10 nm and some agglomerations were also observed. The TEM analysis therefore confirms that the deposited samples are nano-sized particles. A selected smaller area was used to obtain intense reflections which are seen in the SAED images in Fig. 3. The indexing in red colour corresponds to the wurtzite structure of zinc oxide upon doping with barium. The average d-spacing obtained from the visible lattice fringes for the 3%, 5% and 7% were 0.292 nm, 0.270 nm and 0.253 nm respectively. An increase in the grain size of the particles is seen as an increase in the intensity of the ring pattern. The weak diffused rings correspond to smaller grain sizes [37] which were also observed in the TEM images. {{}}

3.2. Surface morphology and chemical compositions

These micrographs showed that the surfaces of BaZnO films improved after the doping process. Relatively varying grain sizes were

Table 1
Crystallographic parameters of undoped ZnO and Ba-doped ZnO.

Ba Concentration	FWHM (°)	D (nm)	d (nm)	ε (x10^{-3})	δ (x10^{-4} nm^{-2})
Undoped	0.1004	82.2167	0.281	1.539	1.48
1 mol%	0.2733	30.4258	0.260	3.841	10.80
3 mol%	0.2510	33.1290	0.260	3.528	9.11
5 mol%	0.2727	30.4955	0.259	3.529	10.75
7 mol%	0.2616	31.7807	0.260	3.685	9.90

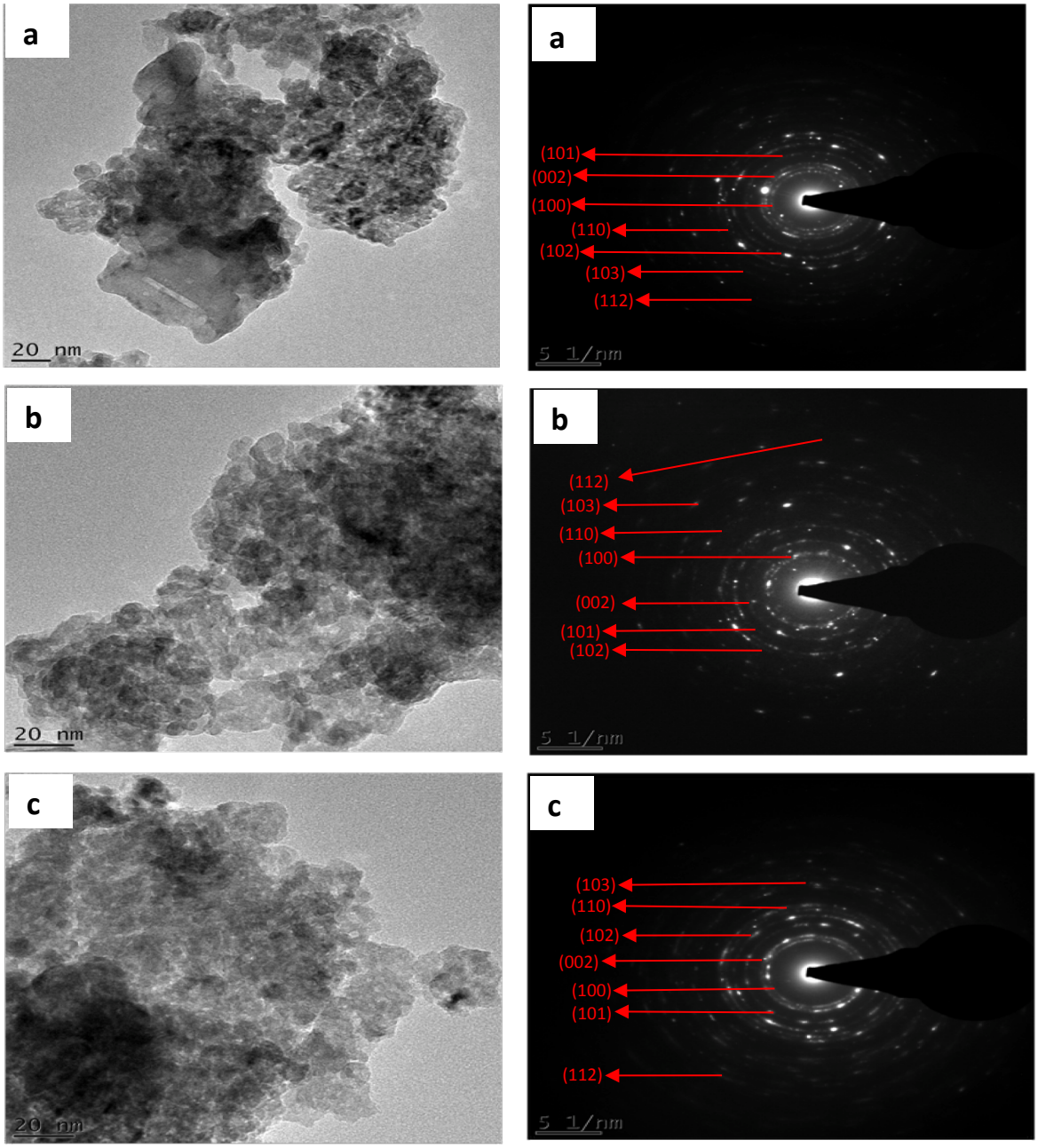

Fig. 3. Low magnification transmission electron micrographs of a) 3% b) 5% c) 7% barium-doped ZnO thin films. Corresponding SAED patterns are shown on the right hand side.

observed upon introduction of different percentages of dopant. Fig. 4(a) shows an arrangement of highly dense and agglomerated undoped ZnO in bud-like form. Introduction of Ba dopant in smaller concentrations (1–3 mol%) produced more evenly dispersed nanostructures with no change in the budlike shape. Further increase in the concentration (5–7 mol%) revealed the formation of nanocapsules.

The number of cycles plays a huge role in the agglomeration rate of the nanoparticles. As illustrated in Fig. 5, sparsely distributed nanostructures were formed during the growth process. Increasing the number of cycles results in more densely packed nanostructure while increasing the film thickness. In our case, 40 cycles produced highly agglomerated nanoparticles with increased sizes at varying dopant concentration.

The compositions of the elements of ZnO films were studied using EDX as shown in Fig. 6. For all samples, zinc element has a higher ratio when compared to oxygen (O) element. The peaks of silicon originated from the glass substrate. The EDX spectra showed the presence of Zn and O which indicates the deposition of ZnO. Apart from the key elemental composition, the appearance of other

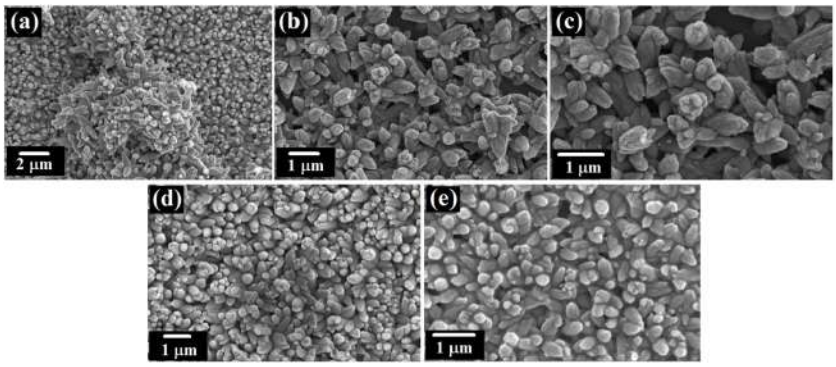

Fig. 4. SEM images of (a) undoped ZnO; Ba doped ZnO at (b) 1 mol%; (c) 3 mol%; (d) 5 mol% and (e) 7 mol%.

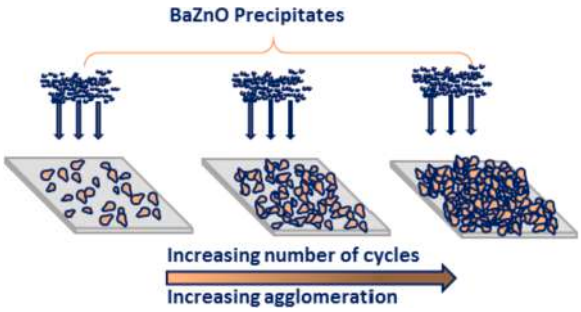

Fig. 5. Growth formation of Ba-doped ZnO nanoparticles using SILAR method.

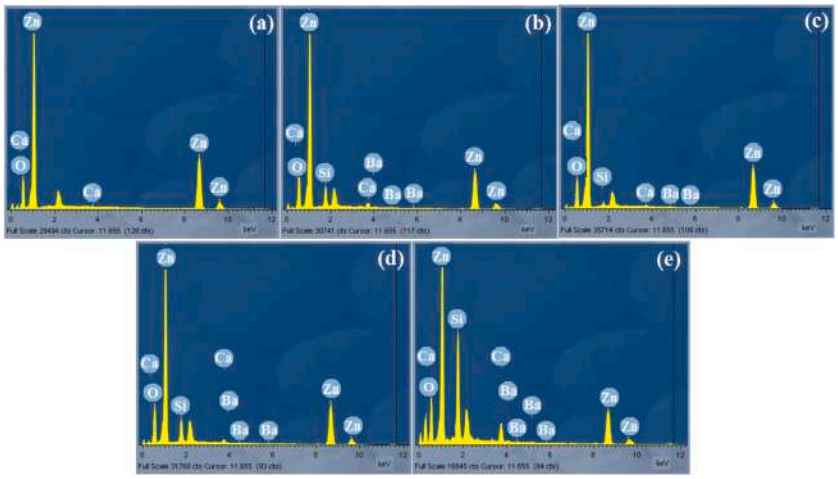

Fig. 6. EDX graphs of (a) undoped ZnO; Ba-doped ZnO at (b) 1 mol%; (c) 3 mol%; (d) 5 mol% and (e) 7 mol%.

elements such as silicon Si, C, and Ca was as a result of the glass substrates and the carbon adhesive used during the sample preparation.

3.3. Optical properties

The undoped ZnO thin film recorded the highest energy band gap value when compared with those doped with 1 mol%, 3 mol%, 5 mol% and 7 mol% as shown in Fig. 7(a–e). As represented in Fig. 7(f), the band gap values of ZnO film decreased with increase in the percentages of doping. This decrease is because the dopant tends to increase the valence band of the ZnO film; thereby minimizing the amount of energy needed by the electrons to jump from the valence band to the conduction band. This decrease in band gap can be used to improve the visible light capturing in solar cell applications [38].

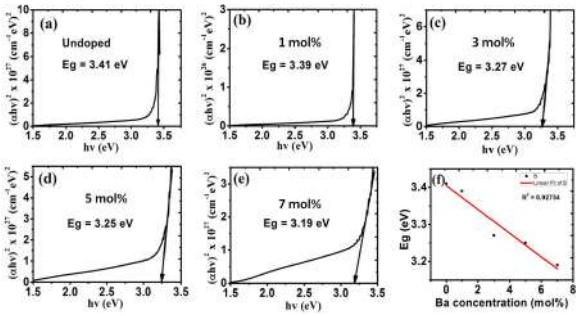

Fig. 7. Energy band gap for (a) undoped ZnO; Ba doped ZnO at (b) 1 mol%; (c) 3 mol%; (d) 5 mol% and (e) 7 mol%. (f) Plot of the decreasing bandgap with increased Ba concentration.

Fig. 8 shows the transmittance curves of the deposited films. The films presented relatively lower transmittance in the visible light region which increased towards higher wavelength regions. The highest transmittance was recorded for the Ba-doped ZnO at 1 mol%. Further increase in the dopant concentration showed a slight decline in the transmittance value because the increased dopant concentration increases the film thickness which hinders maximum penetration of incident light through the deposited films.

The average refractive indices of 2.64, 2.62, 2.63, 2.64 and 2.45 in the visible light region (400 nm–700 nm) were obtained for the undoped ZnO, Ba-doped ZnO at 1 mol%, 3 mol%, 5 mol% and 7 mol% respectively (Fig. 9(a)). It has been reported that doping ZnO with Li using the spray pyrolysis technique produced refractive indices extending from 1.60 to 2.20 at 500 nm wavelength [39]. Fig. 9 (b) shows that the extinction coefficient of the samples increased with an increase in dopant concentration.

The optical absorbance was recorded by using a single beam spectrophotometer from the wavelength ranging from 350 nm to 1000 nm shown in Fig. 10(a). From the graph, it is observed that absorbance of ZnO thin films decreased as the wavelength increased. The absorbance values were calculated with wavelengths in the range of 390 nm–1000 nm in the visible region. The results show that 7 mol % Ba-doped ZnO has the highest absorbance in the visible light region. Fig. 10(b) shows a plot of absorption coefficient (α) versus wavelength. It can be calculated from equation (10) [40]:

$$\alpha = \frac{2.303(A)}{t} \tag{10}$$

Where A is absorbance and t is the film thickness. From the graph in Fig. 10(b), it is observed that there is an increase in absorption coefficient with increased dopant concentration in the visible region.

Fig. 11(a) shows optical reflectance spectra of different samples of ZnO thin films. It is observed that the reflectance of all the deposited thin films is relatively low. The lowest reflectance in the visible light region was observed at the highest Ba concentration (7 mol%).

The change in optical conductivity with photon wavelength showed that the optical conductivity decreased with rise in the photon wavelength in the visible region as seen in Fig. 11(b). There was no observed trend to show the direct effect of increasing dopant concentration on the optical conductivity.

The refractive index values were used to obtain some dielectric properties such as the lattice dielectric constant ε_L and plasma frequency ω_p using the relation in equation (11) [41].

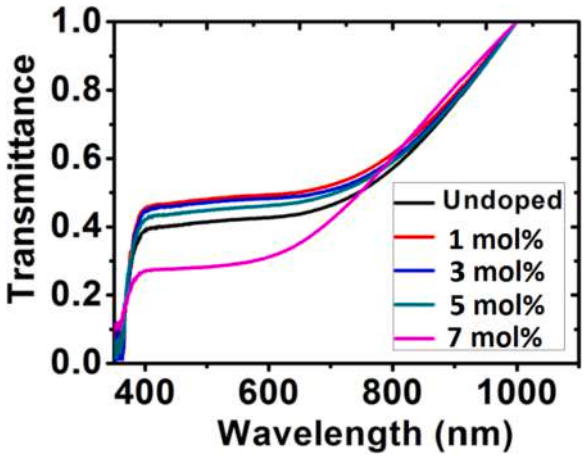

Fig. 8. Transmittance spectra for ZnO and Ba-doped ZnO films.

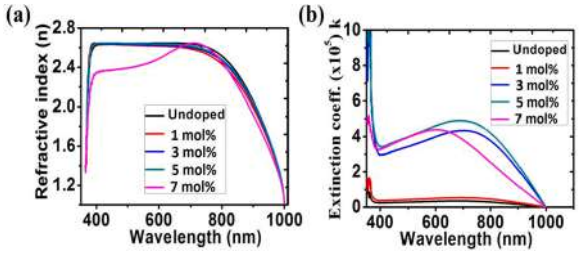

Fig. 9. (a) Refractive index; (b) Extinction Coefficient for ZnO and Ba-doped ZnO films.

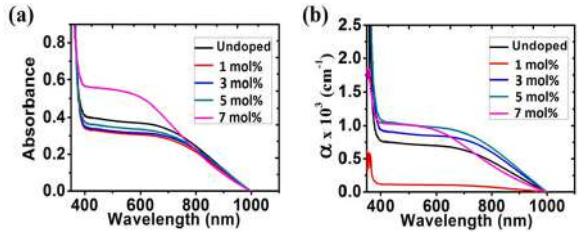

Fig. 10. (a) Absorbance; (b) Absorption coefficient for ZnO and Ba-doped ZnO films.

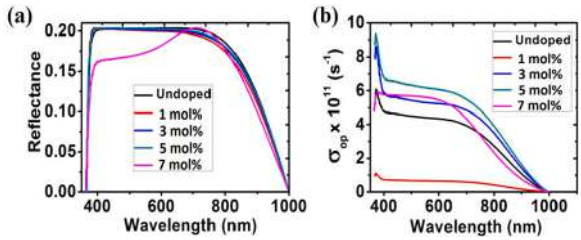

Fig. 11. (a) Reflectance; (b) Optical Conductivity for ZnO and Ba-doped ZnO films.

$$n^2 = \varepsilon_L - \left(\omega_p^2 \Big/ 4\pi c^2\right)\lambda^2 \tag{11}$$

Where, n is the refractive index, ε_L is the lattice dielectric constant, $\omega_p$is the plasma frequency and c is the speed of light. A plot of n^2 against λ^2 as shown in Fig. 12(a) yields ε_L as the intercept while ω_p is calculated from the slope. Table 2 shows the calculated values of these parameters at different dopant concentrations. An increase in Ba concentration led to a near constant lattice dielectric constant while there was a decrease in the plasma frequency. This decrease in plasma frequency implies that there could be a decrease in the charge carrier density as the dopant concentration increases. The plasma frequency indicates the shift to a metallic behaviour from the dielectric property in materials. If the frequency of light incident on the material is greater than the plasma frequency, the light is easily transmitted through the material. Consequently, at lower incident light frequencies, the light will be reflected [42].

The oscillation energy E_o and dispersion energy E_d were obtained using the Wemple and Di Domenico model [43] in equation (12).

$$n^2(h\nu) = 1 + \frac{E_d E_o}{{E_o}^2 - (h\nu)^2} \tag{12}$$

A plot of $(n^2-1)^{-1}$ against $(h\nu)^2$ in Fig. 11(b) produces a slope and intercept of $(E_d E_o)^{-1}$and(E_o/E_d), respectively, from which E_d and E_o were easily calculated and values represented in Table 2. Both the oscillation energy and the dispersion energy decreased with addition of the dopant as compared to the undoped ZnO, and in turn increased with an increased concentration. This is in contradiction with [42] which attributes the decrease in E_o to a decrease in energy band gap E_g.

3.4. Photoluminescence spectroscopy

Photoluminescence studies give insight into intrinsic point defects like oxygen vacancies, interstitial zinc etc in ZnO. Fig. 13 shows the room-temperature photoluminescence (PL) spectra of the undoped and Ba-doped ZnO films under an excitation of 378 nm. As free excitons recombine with each other, emissions due to defects are evident from the three emission peaks seen in the visible region of the PL spectra [44].

The Ba-doped ZnO samples have overlapped spectra patterns in the visible region. The samples show weak emission peaks near

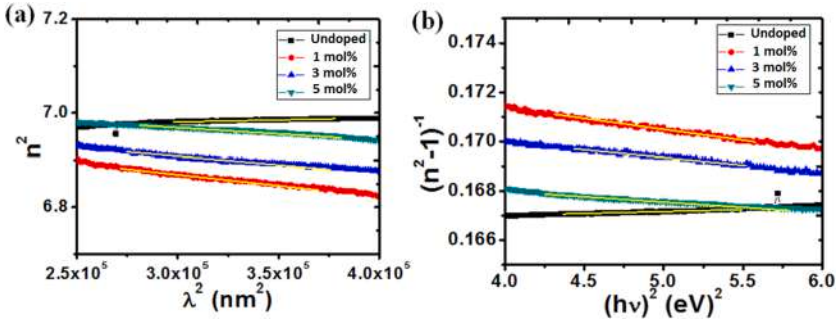

Fig. 12. Plots (a) n^2 vs $\lambda^2$and (b) $(n^2\text{-}1)^{-1}$ vs $(hv)^2$ for calculating the dielectric and optical dispersion parameters, respectively.

Table 2
Summary of the optical constants and dispersion parameters of ZnO and Ba-doped ZnO at different molar concentrations.

Dopant concentration (M%)	N	Eg (eV)	ωp(105 s-1)	εL	Ed (eV)	Eo (eV)
Undoped	2.64	3.41	3.47	6.955	221.04	36.78
1	2.62	3.39	7.40	7.006	78.04	13.63
3	2.63	3.27	6.27	7.012	98.85	17.05
5	2.64	3.25	5.27	7.046	124.67	20.92

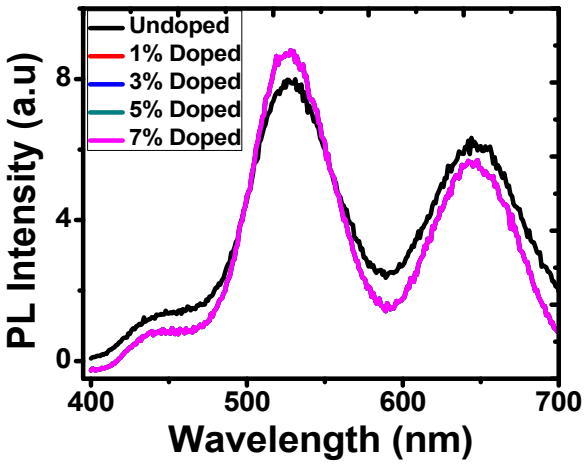

Fig. 13. Photoluminescence spectra of the undoped and Ba-doped ZnO.

435 nm and strong emission peaks at increasing wavelengths. An increase in the luminous intensity at 528 nm could be due to the density of radiative centres and better crystalline nature of the films as confirmed from the SEM and XRD patterns [45]. The decrease in the luminous intensity could be attributed to the size of the ZnO nanoparticles and the doping concentration [46]. The broad emission is due to the surface excitons on the ZnO nanoparticles. The two strong emission bands observed at 528 nm and 642 nm could be due to intrinsic defects like radiative recombination in the oxygen centres and zinc interstitial respectively [44,47]. Emissions could also be due to the transition of electrons from the ionized oxygen vacancies level to the valence band. The overlapped PL spectra for the doped samples follow similar trend with the undoped sample but at varying intensities. The noticeable increase in the PL spectra of the doped samples at 528 nm upon introduction of the Ba dopant as compared to the undoped sample could be likened to increased defect level in the material [44].

4. Conclusion

Undoped and Ba-doped ZnO thin films with different molar concentrations of Ba have been successfully synthesized and characterized. The films showed a preferential orientation of (002) plane, which are polycrystalline in nature as confirmed from XRD studies. The SEM images indicated that the grain size, thus the roughness, increased in proportion with Ba doping level. EDX spectra confirmed the presence of the basic elements deposited. TEM and SAED results confirmed the structural and morphological properties of the films. Optical analysis showed that an optical band gap of ZnO films (undoped and doped) reduced from 3.41eV to 3.19 eV with increased Ba

dopant concentration. When Ba molar concentration was increased, there was a decrease in the plasma frequency which showed a decrease in both the oscillator and the dispersive energies. PL studies confirmed the presence of defects in the undoped and doped ZnO films. The films could find application in optoelectronic devices. In summary, this study reveals the ability to adjust the optical parameters of ZnO by varying the barium dopant concentration.

Acknowledgements

ACN (90406558) and FIE (90407830) cordially acknowledge UNISA for Postdoc and VRSP Fellowship awards, respectively. We are grateful for the grant by TETFUND under contract number *TETF/DESS/UNN/NSUKKA/STI/VOL.I/B4.33*. Finally, we thank Engr. Emeka Okwuosa for substantial funding of April 2014, July 2016 and July 2018 Conference/Workshops on Applications of Nanotechnology to Energy, Health &.Environment conference.

References

[1] O.O. Apeh, U. Chime, S.N. Agbo, S. Ezugwu, R. Taziwa, E. Meyer, P. Sutta, M. Maaza, F.I. Ezema, Properties of nanostructured ZnO thin films synthesized using a modified aqueous chemical growth method, Mater. Res. Express (2018), https://doi.org/10.1088/2053-1591/aadcd6.
[2] M. Nirmala, A. Anukaliani, Structural and optical properties of an undoped and Mn doped ZnO nanocrysatlline thin film, Photonics Lett. Pol. 2 (2010) 189–191.
[3] G. Xiangdong, L. Xiaomin, Y. Weidong, Preparation and characterization of highly oriented ZnO film by ultrasonic assisted SILAR method, J. Wuhan Univ. Technol.-Materials Sci. Ed. 20 (2005) 23–26.
[4] T. Yen, D. Strome, S.J. Kim, A.N. Cartwright, W.A. Anderson, Annealing studies on zinc oxide thin films deposited by magnetron sputtering, J. Electron. Mater. 37 (2008) 764–769.
[5] V. Shelke, B.K. Sonawane, M.P. Bhole, D.S. Patil, Electrical and optical properties of transparent conducting tin doped ZnO thin films, J. Mater. Sci. Mater. Electron. 23 (2012) 451–456.
[6] B. Zhou, A.V. Rogachev, Z. Liu, D.G. Piliptsou, H. Ji, X. Jiang, Effects of oxygen/argon ratio and annealing on structural and optical properties of ZnO thin films, Appl. Surf. Sci. 258 (2012) 5759–5764.
[7] T. Negami, Y. Hashimoto, S. Nishiwaki, Cu (In, Ga) Se2 thin-film solar cells with an efficiency of 18%, Sol. Energy Mater. Sol. Cells 67 (2001) 331–335.
[8] Y. Natsume, H. Sakata, Zinc oxide films prepared by sol-gel spin-coating, Thin Solid Films 372 (2000) 30–36.
[9] X. Wang, W.P. Carey, S.S. Yee, Monolithic thin-film metal-oxide gas-sensor arrays with application to monitoring of organic vapors, Sensor. Actuator. B Chem. 28 (1995) 63–70.
[10] S. Roy, M. Boro, D. Mohanta, A. Choudhury, G.A. Ahmed, Size quantification of sub-micron ZnSe semiconductor particles by laboratory scattering methods, Indian J. Phys. 84 (2010) 705–709.
[11] D.P. Gogoi, G.A. Ahmed, D. Mohanta, A. Choudhury, G.A. Stanciu, Structural and optical properties of Mn doped ZnS semiconductor nanostructures, Indian J. Phys. 84 (2010) 1361–1367.
[12] G. Srinet, R. Kumar, V. Sajal, High Tc ferroelectricity in Ba-doped ZnO nanoparticles, Mater. Lett. 126 (2014) 274–277.
[13] V. Ghafouri, M. Shariati, A. Ebrahimzad, Photoluminescence investigation of crystalline undoped ZnO nanostructures constructed by RF sputtering, Sci. Iran. 19 (2012) 934–942.
[14] D.-S. Kang, K.H. SEOK, M.Y. SANG, J.G. Kim, W.J. Hwang, S.-K. Hong, J.W. Lee, Y.L. JEONG, J.-H. Song, T. Yao, Growth and characterization of zinc oxide nanostructures on (111) silicon substrates with aluminum compound layer, J. Korean Phys. Soc. 53 (2008) 292–298.
[15] G. Patwari, B.J. Bodo, R. Singha, P.K. Kalita, Photoluminescence studies of H2O2 treated chemically synthesized ZnO nanostructures, Res. J. Chem. Sci. 2231 (2013) 606X. ISSN.
[16] K. Sakai, K. Noguchi, A. Fukuyama, T. Ikari, T. Okada, Low-temperature photoluminescence of nanostructured ZnO crystal synthesized by pulsed-laser ablation, Jpn. J. Appl. Phys. 48 (2009), 085001.
[17] Y. Cai, X. Li, Y. Liu, S. Du, P. Cheng, F. Liu, K. Shimanoe, N. Yamazoe, G. Lu, Hollow cylinder ZnO/SnO 2 nanostructures synthesized by ultrasonic spray pyrolysis and their gas-sensing performance, CrystEngComm 16 (2014) 6135–6140.
[18] M.H. Shinen, Preparation of Nano-thin films of ZnO by Sol–Gel method and applications of solar cells Hetrojunction, J. Nat. Sci. Res. 4 (2014) 98–106.
[19] B. Shirdel, M.A. Behnajady, Sol-gel synthesis of Ba-doped ZnO nanoparticles with enhanced photocatalytic activity in degrading Rhodamine B under UV-A irradiation, Optik 147 (2017) 143–150, https://doi.org/10.1016/j.ijleo.2017.08.059.
[20] S. Bagheri, K.G. Chandrappa, S.B.A. Hamid, Facile synthesis of nano-sized ZnO by direct precipitation method, Der Pharma Chem. 5 (2013) 265–270.
[21] S. Thakur, J. Kumar, J. Sharma, N. Sharma, P. Kumar, Structural and optical study of nickel doped ZnO nanoparticles and thin films for dye sensitized solar cell applications, J. Optoelectron. Adv. Mater. 15 (2013) 989–994.
[22] X.D. Gao, X.M. Li, W.D. Yu, Structural and morphological evolution of ZnO cluster film prepared by the ultrasonic irradiation assisted solution route, Thin Solid Films 484 (2005) 160–164.
[23] Y. Shi, K. Wang, Y. Du, H. Zhang, J. Gu, C. Zhu, L. Wang, W. Guo, A. Hagfeldt, N. Wang, Solid-state synthesis of ZnO nanostructures for quasi-solid dye-sensitized solar cells with high efficiencies up to 6.46%, Adv. Mater. 25 (2013) 4413–4419.
[24] P.-Y. Lee, S.-P. Chang, J.-F. Chang, E.-H. Hsu, S.-J. Chang, Highly transparent nanostructured zinc oxide photodetector prepared by successive ionic layer adsorption and reaction, Int. J. Electrochem. Sci. 8 (2013) 6425–6432.
[25] P.S. Kumar, J. Sundaramurthy, D. Mangalaraj, D. Nataraj, D. Rajarathnam, M.P. Srinivasan, Enhanced super-hydrophobic and switching behavior of ZnO nanostructured surfaces prepared by simple solution–immersion successive ionic layer adsorption and reaction process, J. Colloid Interface Sci. 363 (2011) 51–58.
[26] A.U. Ubale, A.N. Bargal, Characterization of nanostructured photosensitive cadmium sulphide thin films grown by SILAR deposition technique, Indian J. Phys. 84 (2010) 1497–1507.
[27] J. Fan, R. Freer, Varistor properties and microstructure of ZnO–BaO ceramics, J. Mater. Sci. 32 (1997) 415–419.
[28] V. Gopala Krishnan, P. Elango, Influence of Ba doping concentration on the physical properties and gas sensing performance of ZnO nanocrystalline films: automated nebulizer spray pyrolysis (ANSP) method, Optik 141 (2017) 83–89, https://doi.org/10.1016/j.ijleo.2017.05.045.
[29] E. Ando, M. Miyazaki, Durability of doped zinc oxide/silver/doped zinc oxide low emissivity coatings in humid environment, Thin Solid Films 516 (2008) 4574–4577.
[30] R. Zamiri, H. Mahmoudi Chenari, H.F. Moafi, M. Shabani, S.A. Salehizadeh, A. Rebelo, J.S. Kumar, M.P.F. Graça, M.J. Soares, J.M.F. Ferreira, Ba-doped ZnO nanostructure: X-ray line analysis and optical properties in visible and low frequency infrared, Ceram. Int. 42 (2016) 12860–12867, https://doi.org/10.1016/j.ceramint.2016.05.051.
[31] T. Minami, H. Sato, S. Takata, N. Ogawa, T. Mouri, Large-area milky transparent conducting Al-doped ZnO films prepared by magnetron sputtering, Jpn, J. Appl. Phys. 31 (1992) L1106.
[32] S. Rani, P. Suri, P.K. Shishodia, R.M. Mehra, Synthesis of nanocrystalline ZnO powder via sol–gel route for dye-sensitized solar cells, Sol. Energy Mater. Sol. Cells 92 (2008) 1639–1645.
[33] W.T. Lim, C.H. Lee, Highly oriented ZnO thin films deposited on Ru/Si substrates, Thin Solid Films 353 (1999) 12–15.

[34] M. Kashif, U. Hashim, M.E. Ali, S.M. Usman Ali, M. Rusop, Z.H. Ibupoto, M. Willander, Effect of different seed solutions on the morphology and electrooptical properties of ZnO nanorods, J. Nanomater. 2012 (2012) 106.
[35] V.D. Mote, Y. Purushotham, B.N. Dole, Williamson-Hall analysis in estimation of lattice strain in nanometer-sized ZnO particles, J. Theor. Appl. Phys. 6 (2012) 6.
[36] P. Bindu, S. Thomas, Estimation of lattice strain in ZnO nanoparticles: X-ray peak profile analysis, J. Theor. Appl. Phys. 8 (2014) 123–134.
[37] R.M. Nagabharana, N. Kiran, P. Guha, B. Sundaravel, U.M. Bhatta, Structural characterization of magnetron sputtered ZnO thin films on Si(100) using RBS, scanning and high resolution transmission electron microscopy methods, Surf. Interfaces 15 (2019) 239–243, https://doi.org/10.1016/j.surfin.2019.03.006.
[38] S.Y. Raghvendra, C.P. Avinash, S. Sharda, Optical properties of emporium doped bunches of ZnO, Chalcogenide Lett. 6 (2009) 233–239.
[39] P. Pushparajah, A.K. Arof, S. Radhakrishna, Physical properties of spray pyrolysed pure and doped ZnO thin films, J. Phys. Appl. Phys. 27 (1994) 1518.
[40] D. Kumar, G. Agarwal, B. Tripathi, D. Vyas, V. Kulshrestha, Characterization of PbS nanoparticles synthesized by chemical bath deposition, J. Alloy. Comp. 484 (2009) 463–466.
[41] K.S. Usha, R. Sivakumar, C. Sanjeeviraja, Optical constants and dispersion energy parameters of NiO thin films prepared by radio frequency magnetron sputtering technique, J. Appl. Phys. 114 (2013) 123501.
[42] N. Khemiri, M. Kanzari, Determination and analysis of optical constants and dispersion energy parameters of Zn (S, O) thin films, Mater. Chem. Phys. 214 (2018) 185–191.
[43] S.H. Wemple, M. DiDomenico Jr., Behavior of the electronic dielectric constant in covalent and ionic materials, Phys. Rev. B 3 (1971) 1338.
[44] K. N'KONOU, M. HARIS, Y. LARE, M. BANETO, K. NAPO, Effect of barium doping on the physical properties of zinc oxide nanoparticles elaborated via sonochemical synthesis method, Pramana 87 (2016) 4, https://doi.org/10.1007/s12043-016-1208-8.
[45] L.F. Koao, B.F. Dejene, H.C. Swart, S.V. Motloung, T.E. Motaung, S.P. Hlangothi, Effect of Tb3+ ions on the ZnO nanoparticles synthesized by chemical bath deposition method, Adv. Mater Lett. 7 (2016) 529–535.
[46] L.F. Koao, B.F. Dejene, H.C. Swart, S.V. Motloung, T.E. Motaung, Characterization of annealed Eu3+-doped ZnO flower-like morphology synthesized by chemical bath deposition method, Opt. Mater. 60 (2016) 294–304.
[47] K. N'Konou, Y. Lare, M. Haris, M. Baneto, K.A. Amou, K. Napo, Influence of barium doping on physical properties of zinc oxide thin films synthesized by SILAR deposition technique, Adv. Mater. 3 (2014) 63–67.